International Journal for Housing Science and Its Applications
Publish August 6, 2025. Volume 46, Issue 3 Pages 4841-4849

https://doi.org/10.70517/ijhsa463414

Fault prediction and anomaly diagnosis of permanent magnet fast ring cabinet based on Bayesian network inference modeling

Chunxiao Li[1,*], Wenxuan Wang[1] and Xin Li[1]
[1] State Grid Cangzhou Electric Supply Company, Cangzhou, Hebei, 061000, China
Corresponding authors: (e-mail: 18031991855@163.com).

Abstract In the field of industrial process control in recent years, fault diagnosis technology has just become a very important and popular research direction. By installing sensors in the permanent magnet fast ring cabinet to collect multi-source data, and using data cleaning and standardization techniques, a fault detection and diagnosis method combining Bayesian inference MCMC and DPMM is proposed. The Bayesian inference MCMC method is the core of this fault correction technique, which is analyzed by comparing the differences between the observed data and various types of fault data. The results show that the CDC and RBC methods do not have the ability to track the fault propagation process, while the method proposed in this paper is able to analyze the different fault variables in the propagation process of faults, which verifies the robustness and practicability of this paper's method from multiple perspectives.

Index Terms fault diagnosis, Bayesian inference, permanent magnet fast ring cabinet, data analysis

I. Introduction

With the economic development and technological progress, the development of ring network cabinet is also very rapid [1], [2]. At present, the operating mechanism of ring network cabinet in distribution room during operation mainly has two kinds of spring operating mechanism and permanent magnet operating mechanism [3], [4]. Statistics show that the failure of the operating mechanism accounts for about 70% of the failure of the whole ring network cabinet, and the permanent magnet mechanism has a higher failure rate in the circuit part due to more electronic components in the driving circuit [5]. Therefore, fault prediction and anomaly diagnosis of the operating mechanism of the ring network cabinet in operation, so as to detect the problems earlier, is of great significance to improve the reliability of the ring network cabinet operation [6], [7].

At present, the research focus on the operation state analysis and fault diagnosis of ring network cabinet and other power equipment is mainly concentrated on fault monitoring, fault diagnosis and fault identification, and the search for convenient, efficient and reliable fault prediction and abnormality diagnosis methods has become a trend [8]-[10]. Tan, L et al [11] proposed a new Adaptive Temporal Neighborhood Preserving Embedding (ATNPE) algorithm for fault detection of cable joints in ring cabinets, which combines approximate linear correlation and temporal neighborhood preserving embedding to improve the robustness and generalization of the model while maintaining the same fault detection rate as the existing models. Baojun, L et al [12] used Neighborhood Persistent Embedding (NPE) algorithm and Internet of Things (IoT) technology to achieve real-time fault detection and monitoring of ring network cabinets in distribution networks. Sălceanu, C. E et al [13] experimentally analyzed the catastrophic effects of arcing inside the compartments of ring mains cabinets, which can occur as a result of malfunctions, abnormal operating conditions, or faults, and pose a danger to the personnel present during the installation. Liu, H et al [14] proposed a fault diagnosis method based on fuzzy granular interval theory for distribution network ring cabinets, which can quickly and accurately identify line faults using only locally measured bus-side voltage and positive current signals. Glowacz, A et al [15] proposed a fault diagnosis technique based on the identification of current signals using a primitive feature extraction method and three classification methods (Bayesian classifier, Linear Discriminant Analysis and Nearest Neighbor Classifier) to identify 100% of four different anomalous states. Sapena-Bano, A et al [16] proposed a fault prediction method based on the harmonic order tracking analysis method for the limitations of the traditional Fourier transform based power equipment such as ring network cabinet in fault prediction and anomaly diagnosis. Lu, W et al [17] proposed a deep neural network fault diagnosis model with domain adaptation, which has high classification accuracy in the target domain, and proposed an optimal hyperparameter exploration strategy for this model. Although a number of methods have been proposed for the research of state analysis and fault diagnosis of power equipment such as ring network cabinets, however, these methods have the disadvantages of large training sample size and high noise. In addition, throughout the previous studies, researchers have focused on the diagnosis and analysis of short-term faults, and there are few reports on the realization of potential anomalies and fault warnings in the long-term operation process.

By collecting and integrating multiple data from the permanent magnet fast ring cabinet, the numerical type data such as temperature, current and voltage are normalized to reflect the equipment status. Then the method of Bayesian inference MCMC combined with DPMM is proposed. The physical law between parameters is used to define the distance function of the parameters to be evaluated, and the distance function is combined into the likelihood function of Bayesian inference to convert the parameter evaluation problem into a maximum likelihood function solution problem. The method proposed in this paper, as well as the traditional method, is applied to numerical simulations and experimental comparative studies.

II. Fault prediction and abnormality diagnosis model of permanent magnet fast ring network cabinet

II. A. Data Acquisition and Preprocessing for Permanent Magnet Fast Ring Cabinet

II. A. 1) Multi-source data acquisition techniques

Multi-source data acquisition technology plays a crucial role in the intelligent identification and fault diagnosis system for permanent magnet fast ring main unit. The system monitors temperature changes in key parts of the ring main cabinet through high-precision temperature sensors with an accuracy of up to 0.1°C in order to effectively capture abnormalities such as overload. Meanwhile, current and voltage transformers and high-definition cameras (with infrared night vision function) are used to collect electrical data and visual information respectively. These devices form a unified data network through IoT technology, which ensures real-time data transmission and accurate summarization, providing comprehensive data support for fault analysis.

II. A. 2) Data cleaning and standardization methods

The first step in the data cleaning process is to deal with outliers in the collected data. Temperature data with readings that deviate from the normal range need to be labeled or corrected based on historical data and equipment characteristics to determine if they are sensor errors or interference. Current and voltage data, on the other hand, are identified and outliers are removed through the statistical 3σ principle. The data are normalized by mapping the temperature data linearly to the 0 to 1 interval, while the current and voltage data are normalized according to the rated values, thus ensuring comparability between different data and improving the processing efficiency of the algorithm and the accuracy of fault diagnosis.

II. B. Bayesian inference models

II. B. 1) Distance function

The parameter evaluation problem of Bayesian inference can be realized by defining the distance function of the parameter to be evaluated, whose distance function generally includes the baseline output and the corrected output. The setting of the distance function of the parameter to be evaluated is crucial, and the parameter evaluation problem can be converted into a maximum likelihood function solution problem by combining the distance function into the likelihood function of Bayesian inference [18]. For air conditioning system failures, the parameters to be evaluated are defined as sensor measurements or equipment failure condition performance magnitudes. Theoretically, the internal correlation between the parameters can be characterized by the physical laws between the parameters, data fitting and machine learning, so as to establish the distance function based on the plausible parameter definitions, the parameter definitions to be assessed, the non-assessment parameter definitions, or the benchmark expansion. Specifically, there exist four common forms of setting the distance function for the parameters to be assessed:

(1) The distance function $D_1(x)$ based on the definition of credible parameters is shown in equation (1), which consists of the baseline output of credible parameters and the corrected output. Credible parameters can often be measured directly, and generally can be considered accurate and credible, such as total energy consumption of air conditioning systems, fan energy consumption, pump energy consumption, outdoor meteorological parameters. As shown in equation (2), the benchmark output YB_1 of the trusted parameter is equal to the measured value of the parameter. And the calibration value YC_1 of the credible parameter consists of the parameter measurement value and the parameter compensation value (i.e., the parameter offset constant), including the measured value of the parameter to be evaluated and its offset constant value, as shown in equation (3).

$$D_1(x) = \sum_{n=1}^{N} \sum_{i=1}^{I} \left(YB_{1,i} - YC_{1,i} \right)^2 \tag{1}$$

$$YB_{1,i} = S_i \tag{2}$$

$$YC_{1,i} = g_1\left(M_1, M_2, \cdots, M_p, x_1, x_2, \cdots, x_q\right) \tag{3}$$

where $D_1(x)$ is the distance function defined based on the plausible parameters; YB_1 and YC_1 are the baseline and corrected outputs of the plausible parameters, respectively; S is the plausible parameter measurement; M is the parameter measurement; and x is the parameter offset constant, which includes the magnitude of the sensor measurement bias and the severity level of the device failure; N and I are the number of parameter measurement datasets and evaluation parameters, respectively; n is the ordinal number of the parameter measurement dataset; i, p and q are the evaluation parameter ordinal numbers; g_1 is the corrected output function defined based on the plausible parameters.

(2) The distance function $D_2(x)$ defined based on the parameters to be evaluated is shown in equation (4). Accordingly, the baseline output value YB_2 of the parameter to be evaluated is defined by the measured value of other parameters and the corresponding offset constant; and the corrected output value YC_2 of the distance function based on the definition of the parameter to be evaluated is composed of the measured value of the evaluated parameter and the offset constant, and its value is usually equal to the cumulative value of the measured value of the evaluated parameter and the offset constant.

$$D_2(x) = \sum_{n=1}^{N}\sum_{i=1}^{I}(YB_{2,i} - YC_{2,i})^2 \tag{4}$$

$$YB_{2,i} = f_2\left(M_1, M_2, \cdots, M_p, x_1, x_2, \cdots, x_q\right) \tag{5}$$

$$YC_{2,i} = g_2(M_i, x_i) \tag{6}$$

where $D_2(x)$ is the distance function defined based on the parameters to be evaluated; YB_2 and YC_2 are the baseline and corrected outputs of the parameters to be evaluated, respectively; and f_2 and g_2 are the baseline output function and corrected output function defined based on the parameters to be evaluated, respectively.

(3) The distance function $D_3(x)$ defined based on the non-evaluated parameters is shown in equation (7). Different from the distance function $D_2(x)$, at this time the parameters to be evaluated are no longer the dependent variables of the benchmark output function, but the independent variables of its benchmark output function. Wherein, the benchmark output value YB_3 of the non-evaluated parameter consists of other parameter measurements including the parameter to be evaluated and the corresponding offset constants; while the corrected output value YC_3 of the distance function defined based on the non-evaluated parameter consists of the non-evaluated parameter measurements and the offset constants, which is usually equal to the cumulative value of the parameter measurements and the offset constants.

$$D_3(x) = \sum_{n=1}^{N}\sum_{i=1}^{I}(YB_{3,i} - YC_{3,i})^2 \tag{7}$$

$$YB_{3,i} = f_3\left(M_1, M_2, \cdots, M_p, x_1, x_2, \cdots, x_q\right) \tag{8}$$

$$YC_{3,i} = g_3(M_i, x_i) \tag{9}$$

where $D_3(x)$ is the distance function defined based on non-evaluated parameters; YB_3 and YC_3 are the benchmark output and corrected output of non-evaluated parameters, respectively; and f_3 and g_3 are the benchmark output function and corrected output function defined based on non-evaluated parameters, respectively.

(4) The distance function $D_4(x)$ based on the benchmark expansion is shown in Equation (10), which is based on the available measurement data, and selectively increases one or more of the above three distance functions in order to expand the number of equations of the parameters to be evaluated in the distance function, and to increase the binding force of the distance function on the parameters to be evaluated, so as to weaken the negative impact of parameter underdetermination on the calibration results. Parameter underdetermination means that the given number of equations is not enough to define all the parameters to be evaluated in the distance function, resulting in the existence of multiple solutions of the equations, which leads to poor calibration results.

$$D_4(x) = \sum_{n=1}^{N}\sum_{i=1}^{1}\left[\left(YB_{1,i} - YC_{i,i}\right)^2 + \left(YB_{2,i} - YC_{2,i}\right)^2 + \left(YB_{3,i} - YC_{3,i}\right)^2\right] \tag{10}$$

where $D_4(x)$ is the distance function of the parameter to be evaluated based on the benchmark expansion.

II. B. 2) Fundamentals of Bayesian Reasoning

The basic principle of Bayesian inference is to derive a set of values such that there is as close a match as possible between the corrected value of the parameter to be corrected and the true value of the parameter to be corrected. The posterior distribution $P(x|Y)$ of the offset constant x of the parameter to be corrected is jointly defined by the full probability function $P(Y)$, the prior distribution $\pi(x)$, and the likelihood function $P(Y|x)$, and the basic mathematical expression is shown in equation (11). Based on the central limit theorem, the prior distribution $\pi(x)$ of each offset constant is defined to obey the normal distribution. Where the full probability function $P(Y)$ is a normalized constant as shown in equation (12). The likelihood function $P(Y|x)$ is usually set as a normally distributed probability density function with zero mean. The distance function $D(x)$ in Eq. (13) represents the difference between the benchmark function and the calibration function.

$$P(x|Y) = \frac{P(Y|x) \times \pi(x)}{P(Y)} \tag{11}$$

$$P(Y) = \int P(Y|x)\pi(x)dx \tag{12}$$

$$P(Y|x) = \frac{1}{\sigma\sqrt{2\pi}} \exp\left[-\frac{1}{2\sigma^2} D(x)\right] \tag{13}$$

where x is the offset constant of the parameter to be corrected; Y is the observation; $P(x|Y)$ is the posterior distribution function of the offset constant; $P(Y)$ is the full probability function; $P(Y|x)$ is the likelihood function of the offset constant; $\pi(x)$ is the prior distribution function of the offset constant; σ is the standard deviation; $D(x)$ is the distance function of the offset constant.

II. B. 3) MCMC algorithm equivalent sampling

In Bayesian inference, the posterior distribution of the parameter to be evaluated is determined by the prior distribution of the parameter to be evaluated, the likelihood function and the full probability function. However, the full probability function in Bayesian inference is a very complex integration problem, which is usually difficult to compute directly [19]. Therefore, in this paper, the MCMC method is used to replace the complex integration problem, and the information of the parameters to be corrected is obtained by equivalent sampling through the MCMC method. That is, when the parameter posterior distribution function is defined, the MCMC sampling algorithm is used to generate equivalent samples of the parameter to be corrected, and to obtain the statistical characteristics of the posterior distribution, such as the mean, median and standard deviation.

II. C.Fault diagnosis method of permanent magnet fast ring cabinet

II. C. 1) Construction of the eigen phase space matrix

Fault diagnosis is actually a pattern recognition problem, and feature extraction and selection is the key to pattern recognition. In order to reflect the operating state of the equipment as comprehensively as possible, the commonly used features for mechanical fault diagnosis are selected from the perspective of time domain and time-frequency domain, and the angular domain features are added based on the motion characteristics of reciprocating compressors. After optimizing the features by using the intra-class distance criterion, 34 optimal features are finally obtained. Obtain N sets of training samples X_i, $i \in [1, N]$ with different types of faults, extract features and construct the feature phase space matrix F_i, $i \in [1, N]$.

$$F_i(a) = \begin{bmatrix} f_{1,1} & \cdots & f_{1,p} \\ \vdots & & \vdots \\ f_{q,1} & \cdots & f_{q,p} \end{bmatrix}_{q \times p} \left(a \in [1, b]\right) \tag{14}$$

where, b is the number of data groups contained in each training sample; $F_i(a)$ is the feature matrix of the a th group of data; $f_{e \times g}$ is the g th feature of the signal of the e th measurement point; q is the number of monitoring points; p is the number of features.

II. C. 2) Model training

After inputting F_i as a training sample for the DPMM, the mean-field variational inference method is used to approximate the posterior distribution $p(W_i \mid F_i, \eta_i, \theta_i)$ of the hidden variables $W_i = \{v_i, \eta_i, Z_i\}$ in the model. After the family of variational distributions is obtained, the lower bound L of $\log p(F_i \mid \theta_i)$ is brought to a local maximum by iterating the variational parameter ε_i, and then the weights and parameters of the distribution components are obtained.

The self-learned statistical distribution model M_i of vibration signals of different faults of machinery using the DPMM method, $i \in [1, N]$ can be expressed as:

$$v_i = \{v_{i,k}\}_{k=1}^{\infty} \mid \alpha \sim Beta(1, \alpha) \tag{15}$$

$$\eta_i = \{\eta_{i,k}\}_{k=1}^{\infty} \mid G_0 \sim G_0 \tag{16}$$

$$Z_{i,n} \mid v_i \sim Mult(\varphi(v_i)) \tag{17}$$

$$F_{i,n} \mid z_{i,n} \sim p\left(F_{i,n} \mid \eta_{i,z_{i,n}}\right) \tag{18}$$

where, η_i and $\varphi(v_i)$ denote the parameter set and weight vector of this distributional model, respectively.

II. C. 3) Calculation of Characteristic Contributions

For a given F_i, first calculate the mean value of each feature parameter therein and obtain a set of feature vectors y_i, and then calculate the posterior probability of y_i in each component of the distribution of M_i separately:

$$p(C_m \mid y_i) = \frac{\varphi(v_i)_m \, p(y_i \mid \eta_{i,m})}{\sum_{m=1}^{K} \varphi(v_i)_m \, p(y_i \mid \eta_{i,m})} \tag{19}$$

where, K is the number of distribution components in M_i.

The similarity of each feature parameter in y_i to $C_{i,m}$ can be expressed as:

$$Md_{i,m} = \left[s^{(v)} (M_{i,m}^{\text{cov}} + \varepsilon I)^{-\frac{1}{2}} (y_i - \mu_{i,m}) \right]^2 \tag{20}$$

According to Eq. (14), the characteristic contribution of each type of fault data is calculated and used as a classification model:

$$R_i = \sum_{m=1}^{K} p(C_{i,m} \mid y_i) Md_{i,m} \left(i \in [1, N] \right) \tag{21}$$

II. C. 4) Fault classification

The feature contribution rate r of the observed data is calculated and compared with each classification model $i \in [1, N]$, and the difference between them reflects the degree of similarity between the observed data and various types of fault data. Since the dimension of the feature contribution rate is high and it is difficult to judge the difference between them by direct observation, a distance-based representation of the degree of difference is proposed:

$$D_i = \sum_{l=1}^{L} (r_l - R_{il})^2 \left(i \in [1, N] \right) \tag{22}$$

where, L is the number of feature types. Expressing the difference between feature contributions as a numerical value enables intuitive and effective fault classification.

III. Numerical simulation and experimental research

III. A. Numerical simulation

III. A. 1) Rapidly changing fault simulation

The fault sample can be written in the following general form:

$$x_f = x^* + \xi_i f \tag{23}$$

where f is the fault amplitude and ξ_i is the direction of the fault, indicating that the fault occurs over variable i.

A total of 1000 fault samples are collected, assuming that the fault occurs over variable 4 and the fault amplitude increases at a faster rate starting from 0. The fault samples can be written in the form of equation (24). The fault amplitudes at the 100th, 200th, 500th and 1000th samples are 0.25, 1, 6.25, and 25, respectively.

$$\begin{aligned} x_f &= x^* + \xi_4 f_4 \\ f_4 &= i^2 / 40000\left(i = 1, 2, 3\cdots, 1000\right) \end{aligned} \tag{24}$$

Firstly, the Bayesian inference MCMC method is utilized to detect 1000 fault samples, and the detection results are shown in Fig. 1, (a) and (b) are the fault detection of 1000 samples and the first 300 samples, respectively. Where Figure 1(b) is an enlarged view from 1-300 samples, the green line indicates the control limit of the integrated detection index φ. It can be seen that the detection indicators show an exponential growth trend, and after 170 samples the detection indicators are almost all located above the control limit, and the process detects faults.

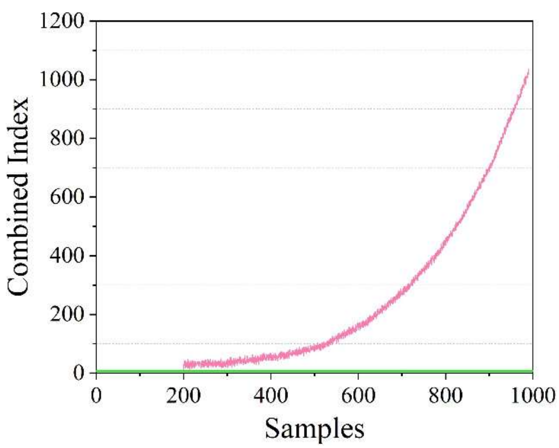

(a) 1000 samples

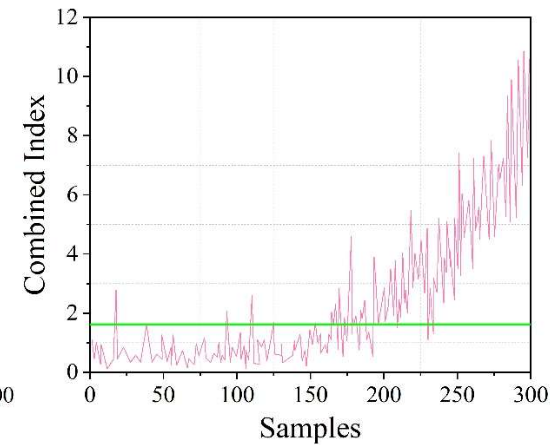

(b) The first 300 samples

Figure 1: Rapid change of mono-transmitter fault detection results

III. A. 2) Slow-change fault simulation

The fault model was changed to be as shown in equation (25) with faults occurring on variable 2 and a total of 1500 fault samples were collected. The fault magnitude increases very slowly and at the 100th, 500th, 1000th and 1500th samples the fault magnitude is 0.005, 0.125, 0.5, and 1.125 respectively.

$$\begin{aligned} x_f &= x^* + \xi_2 f_2 \\ f_4 &= i^2 / 2000000(i = 1, 2, 3..., 1500) \end{aligned} \tag{25}$$

Figure 2 shows the results of fault detection using PCA for 1500 fault samples, and it can be seen that the detection metrics change very slowly and do not exceed the control limits until about 1200 samples.

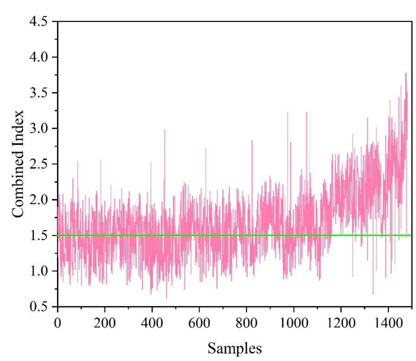

Figure 2: The slow change of the monophone failure test results

The sensitivity of the proposed new method to faults under such slow fault change conditions can be further illustrated by counting the cumulative number of times that variable 2 is diagnosed as a faulty variable over the range of selected samples, as shown in Table 1. If the entire 1500 fault samples are counted, the proposed Bayesian inference based method has 122 more times compared to CDC and 72 more times than RBC. Special observation in the range of 700 to 1200 samples, the proposed method is compared to CDC 56 times more and 21 times more than RBC.

Table 1: The cumulative diagnosis of the failure variable 2 of the slow change

Sample range	CDC	RBC	Proposed method
700-1200	228	263	284
1-1500	572	622	694

From the simulation results, it can be concluded that the proposed method is more sensitive, and due to the cumulative effect on the fault information, it is able to give correct diagnosis results in a shorter time, even before the detection indexes exceed the control limits. While both CDC and RBC have some delay, with CDC having the lowest sensitivity.

III. B. Troubleshooting experiments and analysis

In this simulation experiment, 2 common faults, i.e., blurred output image (fault 1) and insufficient cooling of air cooler (fault 2), are still utilized to verify the fault classification method of the permanent magnet fast grid cabinet. Validity of the method. In this section, contaminated data containing 500 normal samples and 100 fault samples are used as the training set. Then, for both normal and faulty test samples, 50 of them are randomly selected as labeled samples and the remaining are set as unlabeled samples. The test data consists of 300 faulty samples, and the number of retained principal elements A: in both PCA and this paper's model is determined to be 5 by the CPV criterion, and the confidence level of both PCA and this paper's model is set to 99% for the convenience of comparison. And the regulation parameters and 0 in this paper's model are set to 1 based on experience.

First of all, fault 1 is taken as an example for specific analysis and study. the detection results of PCA for fault 1 are shown in Fig. 3. From the figure, it can be seen that when the modeling data used for PCA contains only normal samples, the PCA algorithm has good fault detection performance and can detect most of the abnormal points.

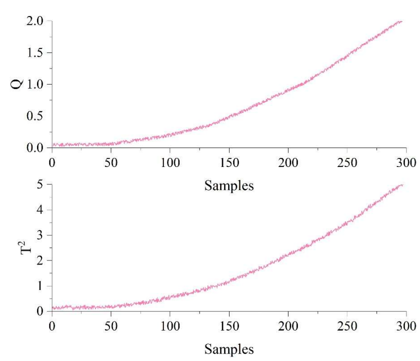

Figure 3: Detection results of fault 1 with pure data by PCA

PCA data for contaminated fault 1 detection is shown in Fig. 4, however, when fault samples are added for modeling, the performance of the PCA model decreases and declines rapidly, and most of the fault sample points are not detected, the main reason is that PCA is an unsupervised method, which is difficult to deal with labeled samples.

The detection results of this paper's method for fault 1 are shown in Fig. 5. In contrast, the method in this paper considers both normal samples and fault samples, and is able to learn the discriminative information of labeled samples while maintaining the global structure of the overall samples, so that it achieves similar fault detection accuracy as PCA for completely normal data, which is much better than that of PCA for contaminated data, and the process data will inevitably be contaminated by fault samples in the process of a complex machine operation. Therefore, the method in this paper is more robust and practical than PCA.

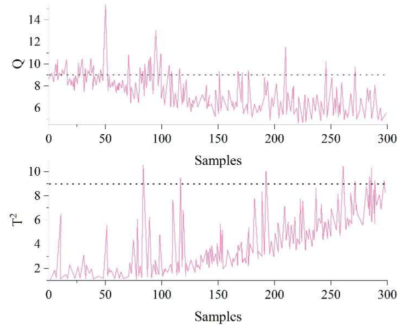

Figure 4: Detection results of fault 1 with polluted data by PCA

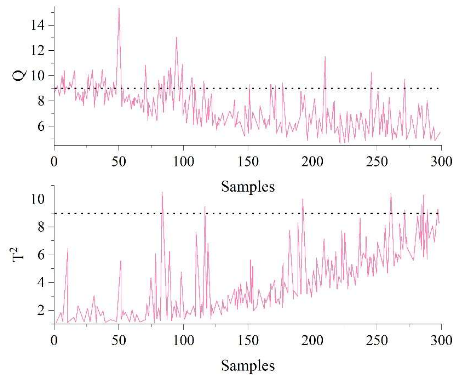

Figure 5: The results of this method are tested for fault 1

In addition, in order to quantitatively evaluate the fault detection accuracy, the quantitative metric of detection performance in this section is chosen as FDRs. then the results of FDRs of the different methods for the 2 faults are shown in Table 2, where the highest FDRs are marked in bold. It can be observed from the table that the proposed method has the highest 100% detection accuracy for fault 2 for both the 2 statistical metrics. Even for fault 1, the detection accuracy of the T_{sem}^2 statistic of this paper's method is only slightly worse than that of PCA for pure fault data (i.e., 97.1% and 100%), and the statistic Q_{sem} of this paper's method still achieves the highest detection accuracy (i.e., 100%). In addition, compared to the comparison algorithms, the model of this paper's method also achieves the highest average FDRs (i.e., 98.55% for T_{sem}^2 and 100% for Q_{sem}) and thus also verifies the superiority of fault detection of this paper's detection model from another perspective.

Table 2: The detection rate of two kinds of failures in different methods

	PCA(Contaminated data)		PCA(Pure data)		This method	
Fault number	T^2	Q	T^2	Q	T_{sem}^2	Q_{sem}
1	3.1	10.8	100	100	97.1	100
2	5.8	1.1	62.4	76	100	100
Mean value	4.45	5.95	81.2	88	98.55	100

IV. Conclusion

In this paper, a fault diagnosis method combining Bayesian inference MCMC and DPMM is proposed, and the diagnostic results are compared by comparing the various types of methods with the characteristic contribution rate of the fault data between. The experimental results show that the proposed method can eliminate the influence of contamination effect and can track the fault propagation process with good applicability. Compared with the comparison algorithms, the method model of this paper also achieves the highest average FDRs (i.e., 98.55% for T_{sem}^2 and 100% for Q_{sem}), and thus also verifies the superiority of fault detection of the detection model of this paper from another perspective.

References

[1] Zhigang, C., Dongchao, L., & Xicai, Z. (2022, September). Research on IoT-based online monitoring technology for ring main unit. In 2022 China International Conference on Electricity Distribution (CICED) (pp. 638-642). IEEE.

[2] Alhanaf, A. S., Farsadi, M., & Balik, H. H. (2024). Fault detection and classification in ring power system with DG penetration using hybrid CNN-LSTM. Ieee Access, 12, 59953-59975.

[3] Zhao, J., Zhang, X., Yang, J., Zhao, S., & Liu, Y. (2022, September). Application Case Analysis of Online Monitoring System for Ring Main Unit Insulation Failure. In 2022 China International Conference on Electricity Distribution (CICED) (pp. 1196-1200). IEEE.

[4] Wagenaars, P., Wouters, P. A., van der Wielen, P. C., & Steennis, E. F. (2010). Influence of ring main units and substations on online partial-discharge detection and location in medium-voltage cable networks. IEEE transactions on Power Delivery, 26(2), 1064-1071.

[5] Bian, F., Zhao, W., Ji, J., Xu, L., Chen, H., & Gao, M. (2020). Mechanism investigation of ring type winding in linear permanent magnet vernier machine for improving force density. IEEE Transactions on Vehicular Technology, 69(3), 2588-2597.

[6] Liu, D., Sun, F., Zhao, C., Ge, Y., & Long, W. (2025). A Novel Resource-Efficient Magnetic Field Calculation Method and Analysis of Magnetic Load Conversion for a Multishaft Ring-Plate Magnet Gear. IEEE/ASME Transactions on Mechatronics.

[7] Yang, Y., Xu, Q., Chen, Y., Yu, T., Fu, G., & Huang, S. (2024). A fast nonlinear equivalent magnetic network model for magnetic jack type control rod drive mechanism in reactor. Progress in Nuclear Energy, 169, 105058.

[8] Choi, S., Haque, M. S., Tarek, M. T. B., Mulpuri, V., Duan, Y., Das, S., ... & Toliyat, H. A. (2018). Fault diagnosis techniques for permanent magnet AC machine and drives—A review of current state of the art. IEEE Transactions on Transportation Electrification, 4(2), 444-463.

[9] He, L., Feng, Y., Zhang, Y., & Tong, B. (2024). Methods for temperature estimation and monitoring of permanent magnet: a technology review and future trends. Journal of the Brazilian Society of Mechanical Sciences and Engineering, 46(4), 174.

[10] Bhattacharya, S. (2015, May). Fault detection on a ring-main type power system network using artificial neural network and wavelet entropy method. In International Conference on Computing, Communication & Automation (pp. 1032-1037). IEEE.

[11] Tan, L., Li, P., Tao, F., Miao, A., & Cao, M. (2020). Cable joint fault detection for the ring main unit based on an adaptive TNPE algorithm. Wiley Interdisciplinary Reviews: Data Mining and Knowledge Discovery, 10(1), e1336.

[12] Baojun, L. (2021, October). Research on NPE Algorithm of Ring Main Unit Fault Detection Based on Internet of Things Technology. In International Conference on Genetic and Evolutionary Computing (pp. 669-678). Singapore: Springer Nature Singapore.

[13] Sălceanu, C. E., Enache, S., Dobrea, C., Iovan, D., Ocoleanu, D., Nicola, M., ... & Ionescu, M. (2024). Experimental Study of the Behaviour of Ring Main Unit-Type Panels in the Event of Internal Arcing in Different Compartments. Energies, 17(11), 2500.

[14] Liu, H., Han, H., Zheng, X., Sun, Y., Su, M., Ling, T., & Liu, X. (2024). Fuzzy granulation interval-based fault diagnosis method for ring-type DC microgrid. IEEE transactions on Smart Grid, 15(4), 3402-3417.

[15] Glowacz, A., Glowacz, W., Glowacz, Z., Kozik, J., Gutten, M. H., Korenciak, D., ... & Carletti, E. (2017). Fault diagnosis of three phase induction motor using current signal, MSAF-Ratio15 and selected classifiers. Archives of Metallurgy and Materials.

[16] Sapena-Bano, A., Pineda-Sanchez, M., Puche-Panadero, R., Perez-Cruz, J., Roger-Folch, J., Riera-Guasp, M., & Martinez-Roman, J. (2015). Harmonic order tracking analysis: A novel method for fault diagnosis in induction machines. IEEE transactions on energy conversion, 30(3), 833-841.

[17] Lu, W., Liang, B., Cheng, Y., Meng, D., Yang, J., & Zhang, T. (2016). Deep model based domain adaptation for fault diagnosis. IEEE Transactions on Industrial Electronics, 64(3), 2296-2305.

[18] N. Pelletier,A. Thiagarajan,F. Durnin Vermette,L. Chang,D. Choo,D. Cerkowniak... & A.J. VandenBygaart. (2025). Approximate Bayesian inference for calibrating the IPCC tier-2 steady-state soil organic carbon model for Canadian croplands using long-term experimental data. Environmental Modelling and Software,190,106481-106481.

[19] Jie Li,Gary Green,Sarah J.A. Carr,Peng Liu & Jian Zhang. (2025). Bayesian Inference General Procedures for A Single-subject Test study. Neuroscience Informatics,5(2),100195-100195.